Feedbacks of Vegetation on Summertime Climate Variability over the North American Grasslands. Part II: A Coupled Stochastic Model

Weile Wang* and Bruce T. Anderson

Department of Geography and Environment, Boston University, Boston, Massachusetts

Dara Entekhabi

Ralph M. Parsons Laboratory, Department of Civil and Environmental Engineering, Massachusetts Institute of Technology, Cambridge, Massachusetts

Dong Huang and Robert K. Kaufmann

Department of Geography and Environment, Boston University, Boston, Massachusetts

Christopher Potter

Ecosystem Science and Technology Branch, NASA Ames Research Center, Moffett Field, California

Ranga B. Myneni

Department of Geography and Environment, Boston University, Boston, Massachusetts

Received 27 January 2006; accepted 2 May 2006

* Corresponding author address: Weile Wang, Department of Geography and Environment, Boston University, 675 Commonwealth Ave., Boston, MA 02215.
E-mail address: wlwang@bu.edu

ABSTRACT: A coupled linear model is derived to describe interactions between anomalous precipitation and vegetation over the North American Grasslands. The model is based on biohydrological characteristics in the semiarid environment and has components to describe the water-related vegetation variability, the long-term balance of soil moisture, and the local soil–moisture–precipitation feedbacks. Analyses show that the model captures the observed vegetation dynamics and characteristics of precipitation variability during summer over the region of interest. It demonstrates that vegetation has a preferred frequency response to precipitation forcing and has intrinsic oscillatory variability at time scales of about 8 months. When coupled to the atmospheric fields, such vegetation signals tend to enhance the magnitudes of precipitation variability at interannual or longer time scales but damp them at time scales shorter than 4 months; the oscillatory variability of precipitation at the growing season time scale (i.e., the 8-month period) is also enhanced. Similar resonance and oscillation characteristics are identified in the power spectra of observed precipitation datasets. The model results are also verified using Monte Carlo experiments.

KEYWORDS: Land–atmosphere interactions; Vegetation feedbacks; Soil water balance

1. Introduction

In the first part of this study (Wang et al. 2006, hereafter W1), statistical techniques are used to detect and analyze the influence of vegetation on climate variability over the North American Grasslands. Results indicate significant Granger causal relationships (Granger 1969; Granger 1980) from lagged anomalies of vegetation activity to variations of summertime precipitation and surface temperature, particularly when time lags are longer than 2 months (W1). That is, vegetation anomalies earlier in the growing season provide unique information (in a statistically significant fashion) regarding climate variability later in summer. The nature of these causal relationships suggests that if mean vegetation anomalies are high (positive) during the preceding months and/or the vegetation anomalies show a decreasing trend, the climatic conditions during the following summer months (July–September) will tend to be drier and warmer (W1). As suggested by the sign of these climate–vegetation interactions, vegetation and precipitation anomalies are also found to have distinct oscillatory variability at growing season time scales (W1; also see below).

A physical mechanism was proposed to explain the statistical results of W1. In an arid/semiarid environment, where soil water storage is limited, initially enhanced vegetation may deplete soil water faster than normal and thus generate negative soil moisture anomalies later in the growing season. The drier soil in turn reduces fluxes of water and latent heat to the atmosphere and leads to lower precipitation and higher temperatures. Because drier soils also force vegetation to decrease, such interactions may generate oscillatory adjustments in the two fields. Part of this mechanism has been suggested by previous studies (e.g., Heck et al. 1999; Heck et al. 2001).

Conceptual models of vegetation–atmosphere interactions (e.g., Brovkin et al. 1998; Zeng et al. 2002; Wang 2004) and soil moisture–atmosphere interactions

(e.g., Rodriguez-Iturbe et al. 1991a; Rodriguez-Iturbe et al. 1991b) have been proposed previously by numerous researchers. Through simplified force-feedback schemes, these models are able to analytically capture many of the complicated dynamical characteristics of the climate system. For instance, analyses of these models indicate that vegetation–atmosphere interactions may lead to multiple stable equilibria of the climate system at long time scales (Brovkin et al. 1998; Zeng et al. 2002; Wang 2004). For each of these long-term equilibria, on the other hand, vegetation–atmosphere interactions also act to resist small (and transient) disturbances to the system and thus to maintain its stability (Brovkin et al. 1998; Alcock 2003). From the perspective of dynamics, this stability suggests that such short-term (e.g., intraseasonal) vegetation–atmosphere interactions may be simplified using linear approximations (Glendinning 1994; also see the appendix). Following this line of thinking, therefore, this paper aims to develop a simple linear model to capture the physical mechanism hypothesized by W1.

The rest of the paper is arranged as follows. Section 2 presents a development of the stochastic model used in our study. Section 3 identifies the model and retrieves the necessary system parameters from the observational datasets; section 4 analyzes the dynamic characteristics of vegetation in the model and discusses how they may regulate the variability of precipitation; and section 5 conducts Monte Carlo experiments to further verify the role vegetation plays in influencing precipitation. Section 6 presents the concluding remarks.

2. Model development

For the proposed mechanism governing vegetation–climate interactions in semiarid grasslands regions, three important components need to be considered: 1) the variability of vegetation (V) driven by available soil moisture (S) (Woodward 1987; Nemani et al. 2003); 2) the balance of soil moisture maintained by precipitation (P) and evapotranspiration (ET) (Wever et al. 2002); and 3) the coupling between soil moisture and precipitation (Koster et al. 2004). When *anomalies* of these fields are considered, these relationships may be formulated in the following linear difference equations (see the appendix for detailed discussions):

$$V'_t = \alpha V'_{t-1} + \beta S'_{t-1}, \tag{1}$$

$$S'_t = S'_{t-1} + P'_t - \mathrm{ET}'_t, \tag{2}$$

$$P'_t = \theta S'_{t-1} + \varepsilon_t, \tag{3}$$

where V', S', P', and ET' represent anomalies of the corresponding variables; ε_t in Equation (3) represents the external precipitation variability, which is assumed to be a random process (i.e., white noise); and α, β, and θ are constant parameters, each of which corresponds to a particular physical process. Specifically, α ($0 < \alpha < 1$) is the persistence rate of vegetation variability, β [normalized difference vegetation index (NDVI)/water] represents the short-term response of vegetation to soil moisture anomalies, and θ ($0 < \theta < 1$) indicates the proportion of soil moisture that contributes to local rainfall.

To formulate the evapotranspiration (ET) term in Equation (2), we assume it is a sum of two components: the evaporation component directly related to soil

moisture (Yamaguchi and Shinoda 2002) and the transpiration component associated with vegetation variability. Therefore, we represent ET as

$$\mathrm{ET}'_t = (1 - \sigma)S'_{t-1} + \frac{1}{\gamma} V'_t, \tag{4}$$

where σ and γ are also two constant parameters. In this way Equation (2) can be rewritten as

$$S'_t = \sigma S'_{t-1} + P'_t - \frac{1}{\gamma} V'_t. \tag{2'}$$

Physically, the parameter σ ($0 < \sigma < 1$) is the persistence rate of soil moisture. The coefficient $1/\gamma$ represents the rate of transpiration associated with unit vegetation anomalies. It is written such that γ has the same units as β (NDVI/water). As will be discussed later, γ can be interpreted as the (potential) long-term response of vegetation to precipitation forcing.

Equations (1), (2′), and (3) represent a stochastic model that describes interactions among anomalies of vegetation, soil moisture, and precipitation in an arid/semiarid environment. Prototypes of these equations can be found in the literature. For example, a similar form of Equation (1) has been used to describe water-related vegetation dynamics in Zeng et al. (Zeng and Neelin 2000; Zeng et al. 1999; Zeng et al. 2002); Equation (2) is derived from the "bucket model" of soil water balance (e.g., Budyko 1956; Manabe 1969); and Equation (3) is based on the formulation of soil moisture–precipitation interactions in Rodriguez-Iturbe et al. (Rodriguez-Iturbe et al. 1991a; Rodriguez-Iturbe et al. 1991b). For this study, these relationships have been simplified such that they can be represented as linear equations with constant parameters [i.e., a linear time invariant (LTI) system]. Nevertheless, the physical meaning of the model and its parameters remains clear from the discussion above. Detailed derivations of the model from representative equations found in the literature are given in the appendix. It should also be noted that in order to keep the model simple and the analysis feasible, we have neglected the influence of temperature variations in this scenario; however, analyses indicate that inclusion of temperature in the model does not qualitatively influence the results discussed below.

To facilitate the comparison with the observed covariability of precipitation and vegetation (W1), the model can be represented in a form that explicitly involves only V and P:

$$V'_t = (\sigma + \alpha - \beta/\gamma)V'_{t-1} - \sigma\alpha V'_{t-2} + \beta P'_{t-1}, \tag{5}$$

$$P'_t = \frac{\theta(\sigma - \beta/\gamma)}{\beta} V'_{t-1} - \frac{\theta(\sigma\alpha)}{\beta} \cdot V'_{t-2} + \theta P'_{t-1} + \varepsilon_t. \tag{6}$$

Thus, Equation (5) describes the variability of vegetation as driven by precipitation (referred to as the *open-loop* model hereafter), Equation (6) represents feedbacks of land surface processes to the atmosphere (referred to as the *feedback* function), and together, Equations (5)–(6) are referred to as the *closed-loop* model. This form of the model will be discussed in the following sections.

3. Datasets and model identification

3.1. Datasets

To retrieve the parameters of the model, we use datasets of precipitation (Xie and Arkin 1997) and NDVI (Tucker 1979; Myneni et al. 1997; Myneni et al. 1998; Zhou et al. 2001), which is a measure of vegetation activity. Both datasets provide monthly measurements at global scales over the period of 1982–2000, and the NDVI dataset is aggregated to match the resolution of the precipitation dataset. They are then compiled to form a panel for the North American Grasslands, which includes about fifty-one $2° \times 2°$ grid points that have the biome type of grasslands (Friedl et al. 2002) and lie within 25°–55°N and 90°–130°W (W1). For both datasets, monthly anomalies are calculated relative to their 1982–2000 climatologies (i.e., long-term mean seasonal cycles), respectively. More details about these datasets can be found in W1.

Another dataset used in this study is the Climate Prediction Center (CPC) U.S. UNIFIED Precipitation dataset (Higgins et al. 2000). This dataset provides monthly (and daily) precipitation measurements from 1948 to 1998 for the continental United States at a spatial resolution of $0.25° \times 0.25°$. There are about 2700 grid points in the domain of the North American Grasslands. Monthly anomalies of this dataset are calculated relative to their 1948–98 climatologies. These anomalies are used to calculate the mean power spectra of precipitation variations over this region, which will be discussed later in the paper.

3.2. Model identification

The form of Equations (5) and (6) readily allows their parameters to be estimated from the observational datasets by the methods of regression. For this purpose, we rewrite the equations as

$$V'_t = A_1 V'_{t-1} + A_2 V'_{t-2} + A_3 P'_{t-1} + \varepsilon_{1t}, \tag{5′}$$

$$P'_t = B_1 V'_{t-1} + B_2 V'_{t-2} + B_3 P'_{t-1} + \varepsilon_{2t}, \tag{6′}$$

where As and Bs represent the corresponding regression coefficients.

We utilize two algorithms, namely, the ordinary least squares (OLS) method and the out-of-sample forecast method (see appendix A of W1), to estimate the regression coefficients of Equations (5′)–(6′) and to test their statistical significance levels. Different from the OLS method, the method of out-of-sample forecast is particularly devised for panel data (Granger and Huang 1997): it examines how well the statistical model can predict the climate/vegetation variability at grid points that are *not* included in the regression (W1); also, the testing statistics are constructed based on the accuracy of the predictions rather than the r^2 of the regressions (W1; Diebold and Mariano 1995). As such, this method helps to avoid spurious fits of the statistical model to the data (Granger and Huang 1997). Nevertheless, consistent regression results are obtained via the two algorithms. For the sake of simplicity, therefore, we mainly discuss the results obtained using the OLS method.

Table 1 gives the regression results of Equations (5′) and (6′). Generally, results indicate that the open-loop model captures the variability of NDVI anomalies

Table 1. Regression coefficients for (a) Equation (7) and (b) Equation (8) estimated from observed precipitation and vegetation (NDVI) for the North American Grasslands. Only regression coefficients that are statistically significant at 95% level are shown here.

(a)

Month	A1	A2	A3	r^2
Jun	1.059	–0.593	0.009	0.61
Jul	1.008	–0.533	0.009	0.64
Aug	0.943	–0.424	0.014	0.80
Sep	0.762	–0.193	0.014	0.77
Oct	0.980	–0.398	0.007	0.70

(b)

Month	B1	B2	B3	r^2
Jun			0.326	0.09
Jul		3.236		0.02
Aug	2.144	–4.306	0.125	0.06
Sep		–2.225	0.1417	0.03
Oct	–8.725			0.07

(Table 1a). The r^2 statistics of the regressions of Equation (5′) are above 60% for all the months from June to October, and as high as 80% in August. All estimates of the regression coefficients (*A*s) are significant ($p < 0.05$) and physically consistent during this period. For example, the signs associated with these coefficients show a regular pattern through the season, such that A_2 is always negative while A_1 and A_3 are always positive. Because A_2 represents $-\sigma\alpha$ [Equation (5)], negative values of this coefficient are consistent with the derivation of the model.

Compared with the open-loop model, identification of the parameters of the feedback equation [Equation (6′)] is much more difficult. The regression results (Table 1b) generally indicate low r^2 values (2%–9%), and the estimates of the coefficients (*B*s) are also scattered: August is the only month in which the three coefficients are statistically significant and have the expected sign (Table 1b). These results reflect the fact that land surface feedbacks are generally weak and can be masked by the stronger internal variability of the atmosphere. Nevertheless, the results of Table 1b still provide a way to estimate all the system parameters.

Ideally, the five system parameters can be retrieved from the coefficients in Equations (5′) and (6′) using the following relationships:

$$\beta = A_3, \tag{7a}$$

$$\theta = B_3 = \beta B_2 / A_2, \tag{7b}$$

$$\alpha = A_1 - (\beta/\theta) B_1, \tag{7c}$$

$$\sigma = -A_2/\alpha, \quad \text{and} \tag{7d}$$

$$\gamma = \beta/(\sigma + \alpha - A_1). \tag{7e}$$

Here, the parameter θ can only be estimated from the feedback equation [Equation (6′)]. Based on Equation (7b) and the results of Table 1b, this parameter is

estimated to be about 0.13–0.15 for August and September, and may be as high as 0.33 in June.

The other four parameters (α, β, σ, and γ) are contained in both the open-loop model and the feedback equation. Because the influence of precipitation on vegetation variability is much stronger than the influence of vegetation upon precipitation, we try to estimate these parameters mainly based on the regression results of the open-loop model (Table 1a). However, because Equation (5′) has only three coefficients (A_1–A_3), the four parameters are underdetermined by the open-loop model itself. To fully retrieve them, therefore, we either need to take into account the feedback equation [Equation (6′)] or make an a priori estimate for one of the parameters (see below).

Table 2 shows the estimated values of the five system parameters based on the regression results for August, in which the precipitation–vegetation interactions are most evident (Table 1). As shown, the estimated persistence rate of NDVI anomalies (α) is about 0.70, and the persistence rate of soil moisture (σ) is about 0.60 (Table 2). We also make estimates for these parameters by arbitrarily setting σ to 0.6~1.0 at an interval of 0.1; correspondingly, α decreases from about 0.7 to about 0.4. Nevertheless, we find that these different estimates do not affect the overall characteristics of the model because the combination of the two will still give the same coefficients for Equation (5) and similar coefficients for Equation (6). Therefore, we use the estimates in Table 2 as typical parameters to illustrate the characteristics of the model in the following sections. When it is necessary, we will also discuss how different values of the parameters may induce additional variability as a means of interpreting the characteristics in a physically meaningful way.

4. Model analysis

The regression results of the last section (Table 1) indicate that the open-loop model captures the variability of vegetation driven by precipitation. First, we will diagnosis this model in order to investigate and interpret the dynamics of the vegetation variability. Then we will study how vegetation signals may modulate the variability of precipitation when they propagate to the atmosphere by analyzing the feedback equation [Equation (6)]. Finally, we will try to identify some of the simulated characteristics within the corresponding observed precipitation datasets in order to provide additional evidence for the hypothesized vegetation–precipitation feedbacks contained in the model.

4.1. Open-loop model

As a first check for the open-loop model, we use it to simulate the observed vegetation variations. That is, given known observed precipitation information and

Table 2. System parameters used in the open- and closed-loop models for the North American Grasslands.

α	β	σ	γ	θ
0.703	0.014	0.603	0.039	0.125

two initial values of NDVI, Equation (5) is used to predict observed vegetation variations for the rest of the growing season. Figure 1 shows the results of the simple simulation. Generally, the simulated NDVI evolves with the observed time series, resulting in good agreement between the two (Figure 1). As shown, although the input precipitation signal is fairly noisy, vegetation over the midlatitude grasslands has lower-frequency variations and an apparent oscillatory component, as suggested by W1 (Figure 1).

These dynamic characteristics of the model can be quantified by the frequency response functions of the system (Figure 2), which describes the magnitudes and phase angles of the outputs (NDVI) relative to the sinusoidal inputs (precipitation) at different frequencies. For the convenience of comparison, the gain function (Figure 2a) is normalized by the input gain factor [i.e., β in Equation (5)], such that a 0-dB value suggests that unit variance in precipitation generates unit variance in NDVI. (Such normalization will be used for discussions throughout the paper unless otherwise specified.)

The normalized gain function (Figure 2a) indicates "red" responses of NDVI to precipitation forcing. The magnitude of NDVI is positive (~6 dB) at longer time scales (i.e., periods longer than 8 months) but decreases to negative values (about

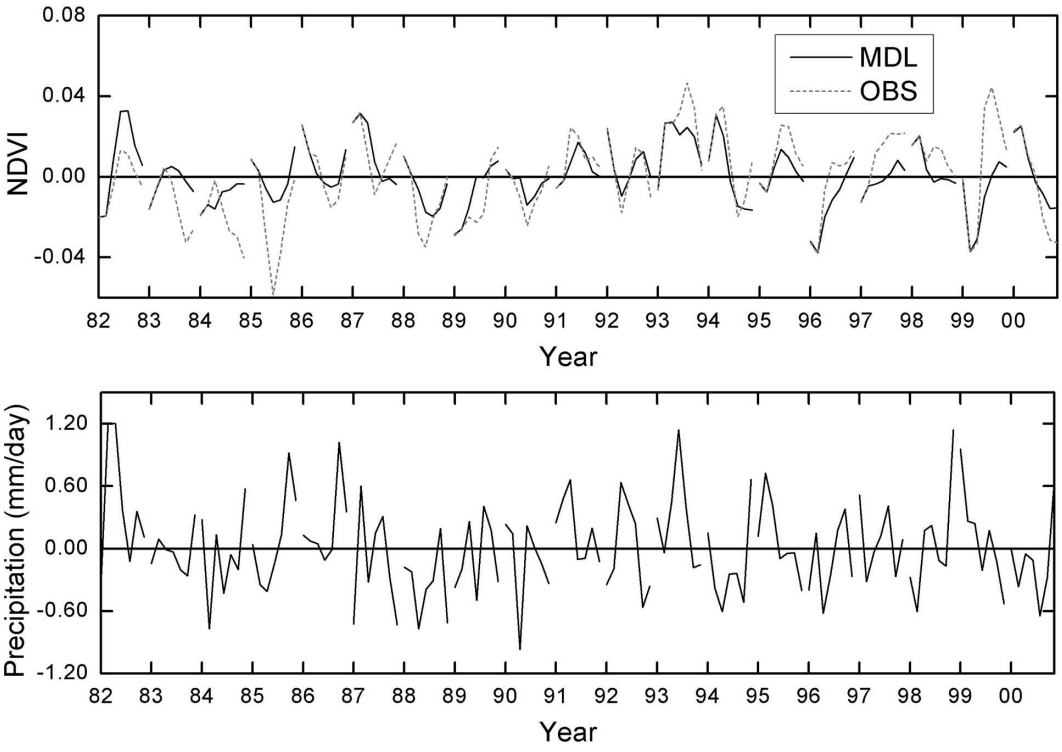

Figure 1. (top) NDVI anomalies simulated with the open-loop model (upper, dark), and the observed NDVI (upper, gray). (bottom) Precipitation anomalies used in the simulation. The simulation uses the first two observed NDVI values of each growing season as initial values and is forced by the precipitation anomalies during the course of the season.

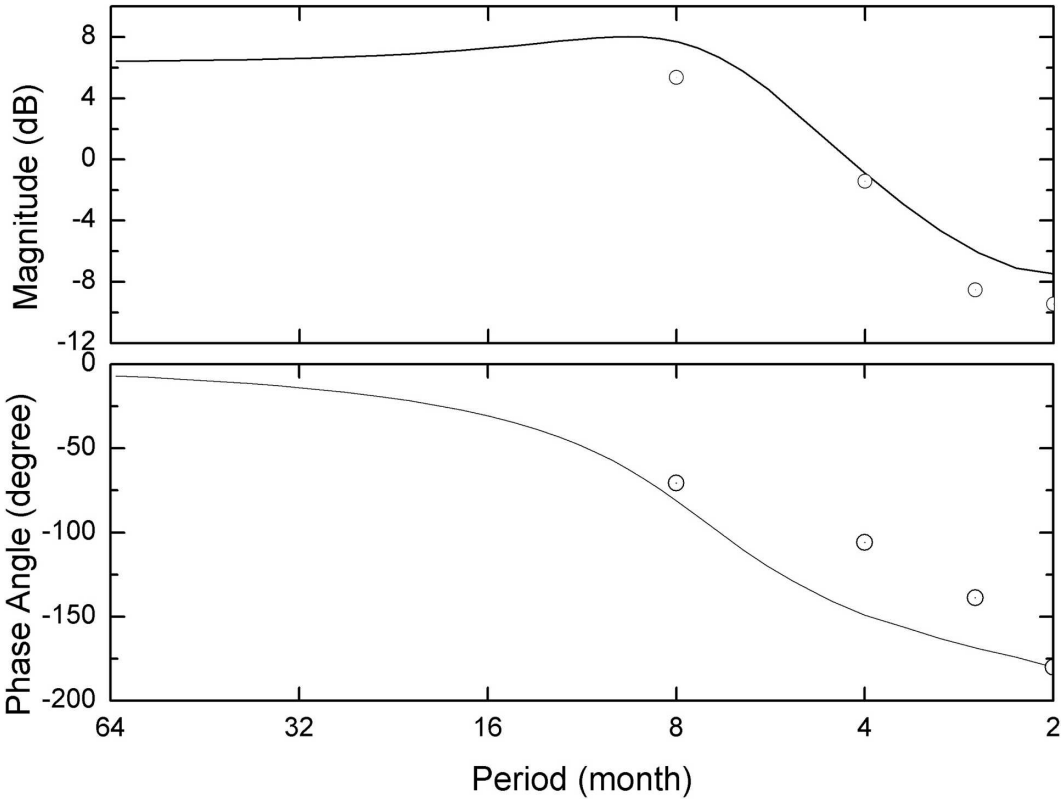

Figure 2. System response functions of NDVI as driven by precipitation (open-loop model). (top) Gain functions; (bottom) phase function. The discrete points ("o") show the estimates from the observed data (taken from W1).

−7 dB at the 2-month period) as the time scales become shorter. Correspondingly, the phase lag between NDVI and precipitation is small at longer time scales but decreases to −180° at the 2-month period (the negative sign indicates that NDVI lags precipitation). The transitions of the magnitude and the phase functions occur at about the 8-month period, where the magnitude peaks (~8 dB) and the phase lag is about −90° (Figure 2), indicating that the system has intrinsic oscillatory variability at this frequency range (Reid 1983). Figure 2 also indicates that the spectral characteristics of the model (line plots) are consistent with those independently estimated from observations only (dot plots; also see W1).

Explanations for these frequency characteristics are provided by the derivation of the model. For example, Equation (1) indicates that vegetation has a "memory" (given by the persistence rate α) of soil moisture variations, and soil moisture itself represents an accumulating process of precipitation [Equation (2)]. Both mechanisms act as low-pass filters to remove transient variations from the input precipitation signals. In addition, Equation (1) indicates that soil moisture surplus promotes vegetation growth; however, Equation (2) indicates that vegetation depletes soil water. The interaction between these two equations therefore can lead to oscillatory adjustments in the vegetation field.

A quantitative interpretation of the red responses of vegetation and its oscillatory variability can also be obtained by analyzing the analytical solution of the model explicitly. As represented by Equation (5), the open-loop model is essentially a second-order difference equation. General solutions to such an equation are determined by its two characteristic roots (or eigenvalues):

$$\lambda_{1,2} = \frac{(\sigma + \alpha - \beta/\gamma) \pm \sqrt{\Delta}}{2}, \tag{8}$$

where

$$\Delta = (\sigma + \alpha - \beta/\gamma)^2 - 4\sigma\alpha. \tag{9}$$

When the characteristic roots have complex components ($\Delta < 0$), this system will have oscillatory variability.

With the estimated α, β, σ, and γ values (Table 2), it can be shown that Equation (8) gives two complex characteristic roots at $\exp(-0.43 \pm i0.76)$. The imaginary part of the exponential indicates an oscillation frequency at 0.76 (radian/month), or equivalently at a period of 8.25 months, which is consistent with the estimated value here and in W1. The real part of the exponential is negative and indicates that the system is stable. Hence, the magnitude of the oscillatory variations will decay at the rate of $e^{-0.43}$ (i.e., $e^{-1/2.3}$, or 0.65) per month; in other words, the time constant of the decay process is about 2.3 months.

The oscillatory decaying adjustments of the open-loop model are represented by its impulse-response function (Figure 3), which examines the output signals of the system when a unit precipitation anomaly is input at the initial time (i.e., $P = 1$ at $t = 0$, and $P = 0$ for $t > 0$). Figure 3 shows that the positive response of

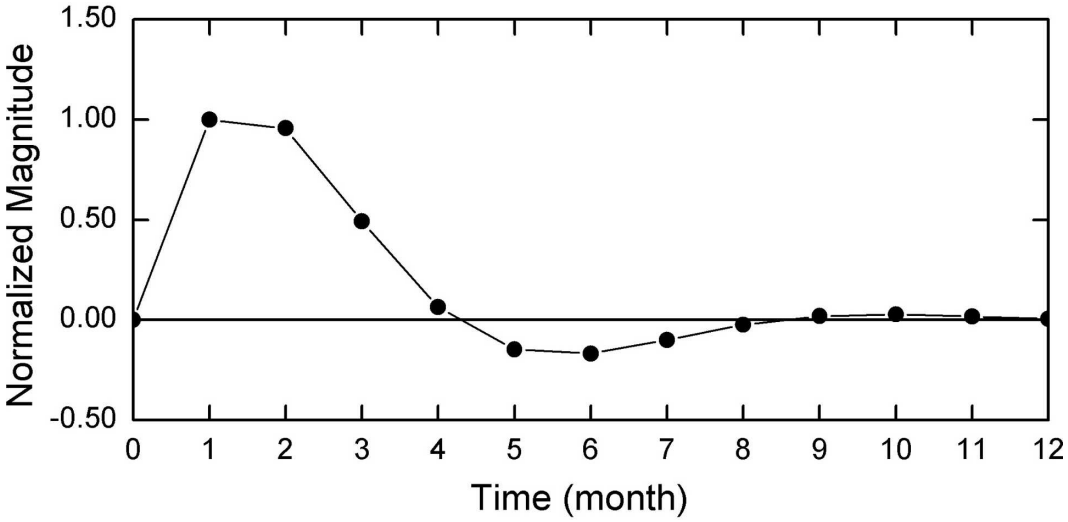

Figure 3. The oscillatory decaying process of NDVI's response to an impulse input of precipitation at time $t = 0$ (open-loop model). The magnitude of NDVI is normalized by the factor β.

vegetation arises in the next month ($t = 1$) and lasts for 4 months (with decreasing magnitudes); the response then switches to the negative phase ($t = 5 \sim 8$), representing the first cycle of the oscillation (Figure 3).

The above analyses all suggest that the model system has a preferred response at low frequencies and that vegetation–soil moisture interactions within the model promote oscillatory behavior. These characteristics of vegetation variability can in turn be physically interpreted using the system parameters (i.e., α, σ, β, and γ) of the model itself. To interpret the red spectra of vegetation, we first check the stability of the system (which as discussed above indicates a stable evolution as opposed to an unstable evolution). By plugging two constant values for precipitation (P_s) and vegetation (V_s) into Equation (5), we find that

$$V_s' = \gamma^* P_s', \tag{10a}$$

where

$$\gamma^* = \frac{\gamma}{[1 + (1 - \sigma)(1 - \alpha)\gamma/\beta]}. \tag{10b}$$

Here, γ^* describes the long-term relationship between vegetation and precipitation, and it is related to the system parameter γ. To see this, note that γ^* is equal to γ when σ is 1 [Equation (10b)]. Because a value of 1 for σ means that all water loss is transpired through vegetation [Equation (2′)], γ describes the *potential* long-term response of vegetation to precipitation, that is, a situation in which vegetation continues to grow until it utilizes all available moisture. On the other hand, as indicated by Equation (1), the rate of vegetation production is determined by the short-term response coefficient β. Therefore, the ratio of β/γ gives a measure of the rate at which vegetation reaches its (potential) equilibrium with precipitation. Given the estimates of the system parameters (Table 2), the value of β (0.014) is about one-third of γ (0.039) and less than one-half of γ^* (~0.030). This means that it takes some time for vegetation to fully respond to precipitation forcing. Therefore, vegetation responds more readily to persistent precipitation variability at longer time scales, producing the red system response function.

In addition we can use Equation (9) to investigate the oscillatory variability of the open-loop system, which is determined by the values of σ, β/γ, and α. As discussed above, when β/γ is high, vegetation production is fast and soil water is consumed rapidly. At the same time, because persistent vegetation anomalies also consume water, vegetation must decay quickly (i.e., α must be small) to avoid negative soil moisture anomalies from being generated. Clearly this process is also regulated by the soil moisture persistence rate σ, which indicates the proportion of soil moisture subject to the influence of vegetation (see below).

We use σ to normalize α and β/γ, and rewrite Equation (9) as follows:

$$\Delta = \sigma^2[(1 + \alpha^* - \beta^*/\gamma^*)^2 - 4\alpha^*], \tag{9′}$$

where

$$\alpha^* = \frac{\alpha}{\sigma}, \quad \beta^*/\gamma^* = \frac{\beta/\gamma}{\sigma}.$$

As such, the oscillatory/nonoscillatory domain of the system can be determined on the $\alpha^* - \beta^*/\gamma^*$ plane (Figure 4). To simplify the discussion, we first consider the

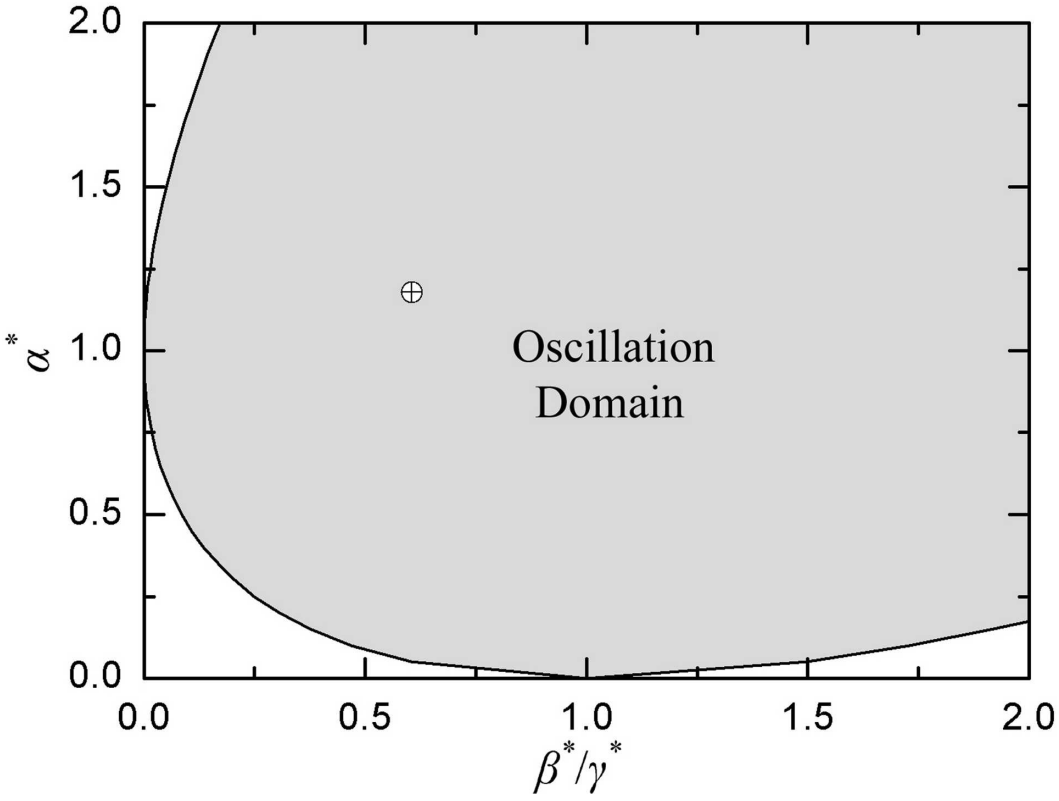

Figure 4. Subdomains of oscillatory (gray) and nonoscillatory (white) variability of the open-loop model on the α^*–β^*/γ^* plane (Equation (9′)). The small circle ("o") indicates the location of the observed system on this plane.

case when σ is 1, and the values of α^* and β^*/γ^* (the same as α and β/γ) are between 0 and 1. In these ranges, the system is nonoscillatory *only* if vegetation has short memory (e.g., α^* is close to 0) or it reaches its steady state slowly enough (i.e., β^*/γ^* is close to 0; Figure 4). When σ is less than 1, the impact of vegetation on soil moisture variability decreases. Therefore, the nonoscillatory domain is also present in the range where α^* or β^*/γ^* is larger than 1 (Figure 4). In either case, however, Figure 4 indicates that for most values of the system parameters, oscillations are likely to be an intrinsic property of the soil moisture–vegetation system.

4.2. External disturbance to vegetation

In addition to precipitation, other external disturbances can also influence vegetation variability. Such disturbances may include climate factors (e.g., temperature, solar radiation, etc.) or nonclimatic factors (e.g., fire, pest, and human activity). To account for the influence of these processes, we introduce an external input term e_t to Equation (1), such that

$$V'_t = \alpha V'_{t-1} + \beta S'_{t-1} + e_t. \qquad (1')$$

If we assume that e_t is independent of the precipitation forcing, the variability of vegetation induced by e_t can be described by

$$V'_t = (\sigma + \alpha - \beta/\gamma)V'_{t-1} - \sigma\alpha V'_{t-2} + e_t - \sigma e_{t-1}. \quad (5'')$$

Because Equation (5″) has the same characteristic equation as Equation (5), the general solutions to this equation have the same properties (i.e., stability and intrinsic oscillations) as discussed before. However, because there is no input of water in Equation (5″), the negative effects of e_t on soil moisture will generate opposing vegetation anomalies [i.e., σe_{t-1} in Equation (5″)] in the following months to counter any initial disturbances. This is illustrated by the impulse-response function (Figure 5). As shown, when e_t induces a unit positive vegetation anomaly at the initial time ($t = 0$), it rapidly decreases to a negative value in 2 months ($t = 2$) and remains negative in the following four months ($t = 2 \sim 5$).

Equation (5″) allows us to explicitly investigate the vegetation variability that is responding to soil moisture variations as opposed to precipitation variations. To denote the fraction of the vegetation variations that is related to soil moisture, we define an additional variable, V'_{soil}, such that

$$V'_{\text{soil}} = V'_t - e_t. \quad (11)$$

The spectral responses of V'_t and V'_{soil} to external disturbances of e_t are illustrated by the corresponding system functions (Figure 6). As shown, the magnitude of V'_t is slightly negative at low frequencies (e.g., −1.4 dB at the 64-month period); at the same time, the magnitude of V'_{soil} is slightly positive (about 2 dB at the 64-month period), but the phase angle is 180°, just opposite that of V'_t. These results suggest that if vegetation growth is initially positive (but there is no corresponding increase in the water supply), the soil will become drier and generate opposing vegetation

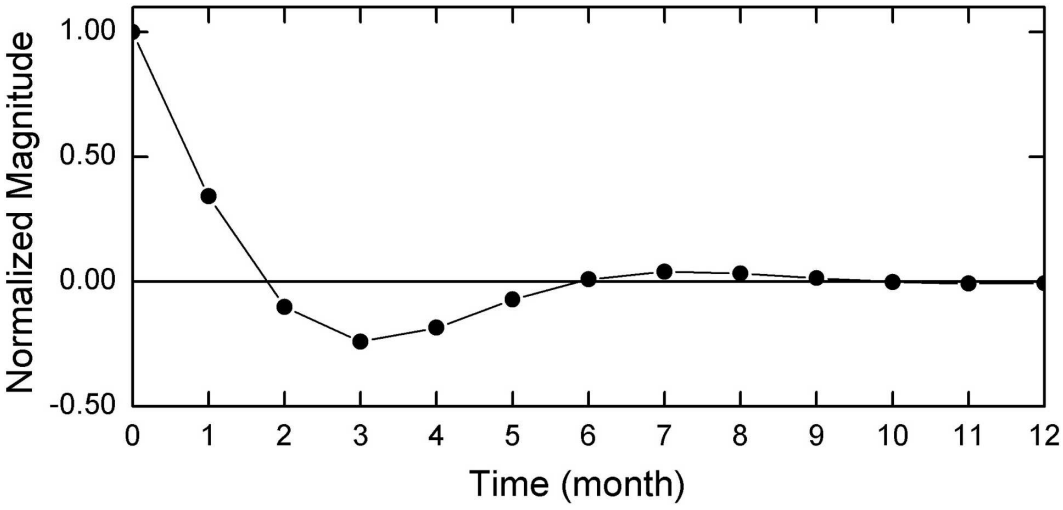

Figure 5. The oscillatory decaying process of NDVI's response to an impulse input of external vegetation disturbance at time $t = 0$ (open-loop model).

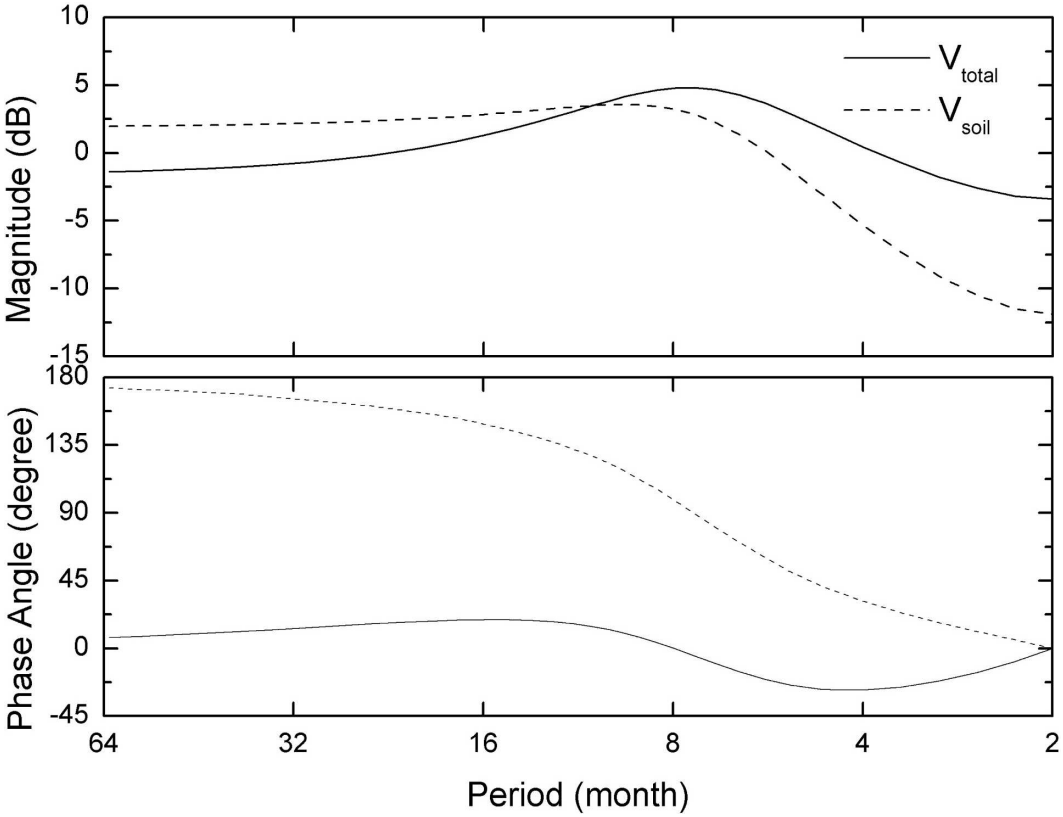

Figure 6. System response functions of NDVI as driven by external vegetation disturbances (open-loop model). The solid line shows the total output of NDVI (V_{total}), while the dashed line shows the portion of NDVI variations associated with soil moisture (V_{soil}).

anomalies (V'_{soil}) to cancel the input. As a result, we get an output of V'_t lower (−1.4 dB, or 0.85) than the input.

4.3. Closed-loop model

Because interactions between vegetation and soil moisture have distinct dynamic characteristics (e.g., Figure 2 and Figure 6), when such signals feed back to the atmosphere [Equation (3) or Equation (6)], they will leave their spectral signatures on the variability of precipitation (Delire et al. 2004). This hypothesis is verified by the spectral characteristics of the closed-loop model.

Figure 7 shows the frequency-response functions of the output precipitation [i.e., P'_t in Equation (6)] relative to the "original" precipitation forcing [i.e., ε_t in Equation (6)]. Overall, it indicates slight but clear red variability of P'_t. The magnitude is slightly enhanced (0.7 dB) at low frequencies but damped (−0.6 dB) at high frequencies, and the transition occurs at about the 8-month period, where the magnitude has a peak of about 1.5 dB (Figure 7). The phase function indicates that P'_t varies almost in phase with ε_t at both high and low frequencies, and the phase lag is also small at transition frequencies (~13°; Figure 7).

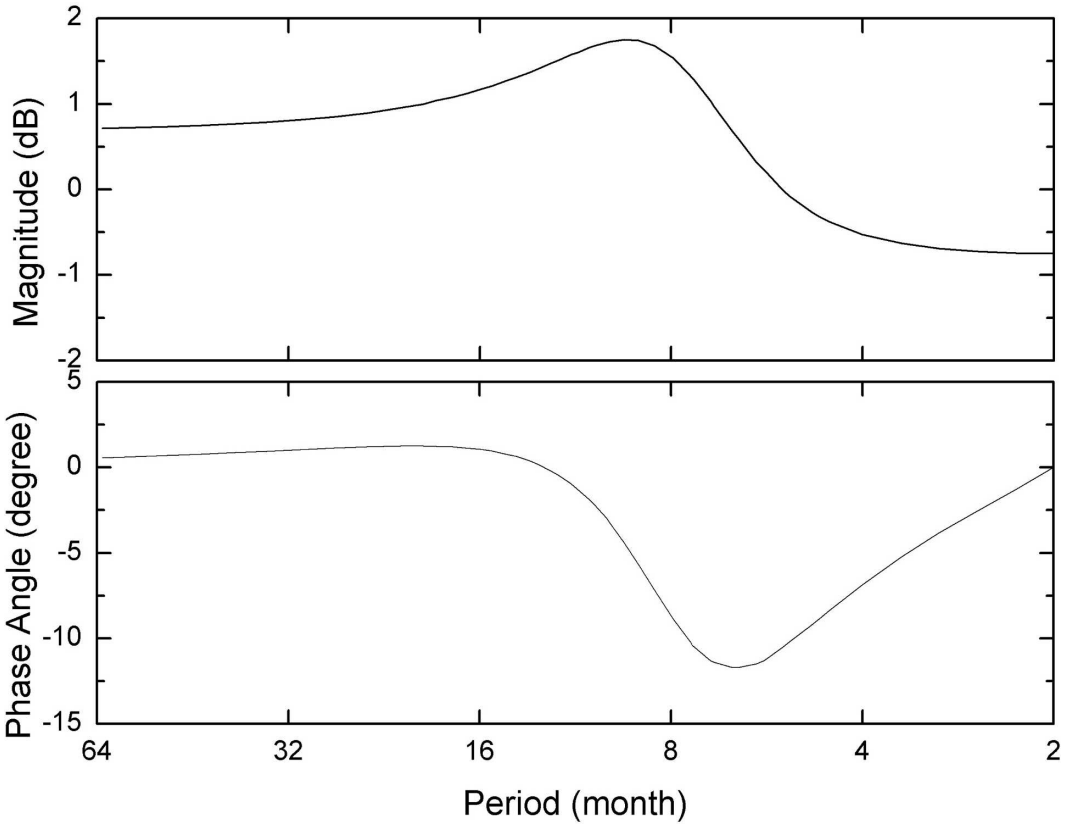

Figure 7. System response functions of precipitation as driven by external precipitation variations (closed-loop model). (top) Normalized gain functions; (bottom) phase function.

The frequency responses of P_t' in Figure 7 have a clear association with the corresponding characteristics of vegetation (Figure 2). Qualitatively, as vegetation varies synchronously with precipitation at low frequencies (Figure 2), the corresponding transpiration anomalies induce water vapor anomalies with the "correct" sign to reinforce the variations of precipitation (Figure 7); on the other hand, because vegetation lags precipitation by almost 180° at high frequencies (Figure 2), the corresponding transpiration anomalies induce water vapor anomalies with the opposite sign, which in turn cancel a portion of the precipitation variability (Figure 7). At the intermediate frequencies where the land surface processes have intrinsic oscillations, the oscillatory variability of precipitation is further enhanced (Figure 7).

Frequency-response functions are also calculated for precipitation as it is driven by external vegetation disturbances [i.e., e_t in Equation (1′) or Equation (5″); Figure 8]. Again, the gain function of precipitation shows a red spectrum that has enhanced (10 dB) magnitudes at low frequencies and damped (about −10 dB) magnitudes at high frequencies, with the transition occurring at about the 8-month period (Figure 8). The phase function indicates that the responses of precipitation are opposite to the external forcing e_t at low frequencies, which is related to the

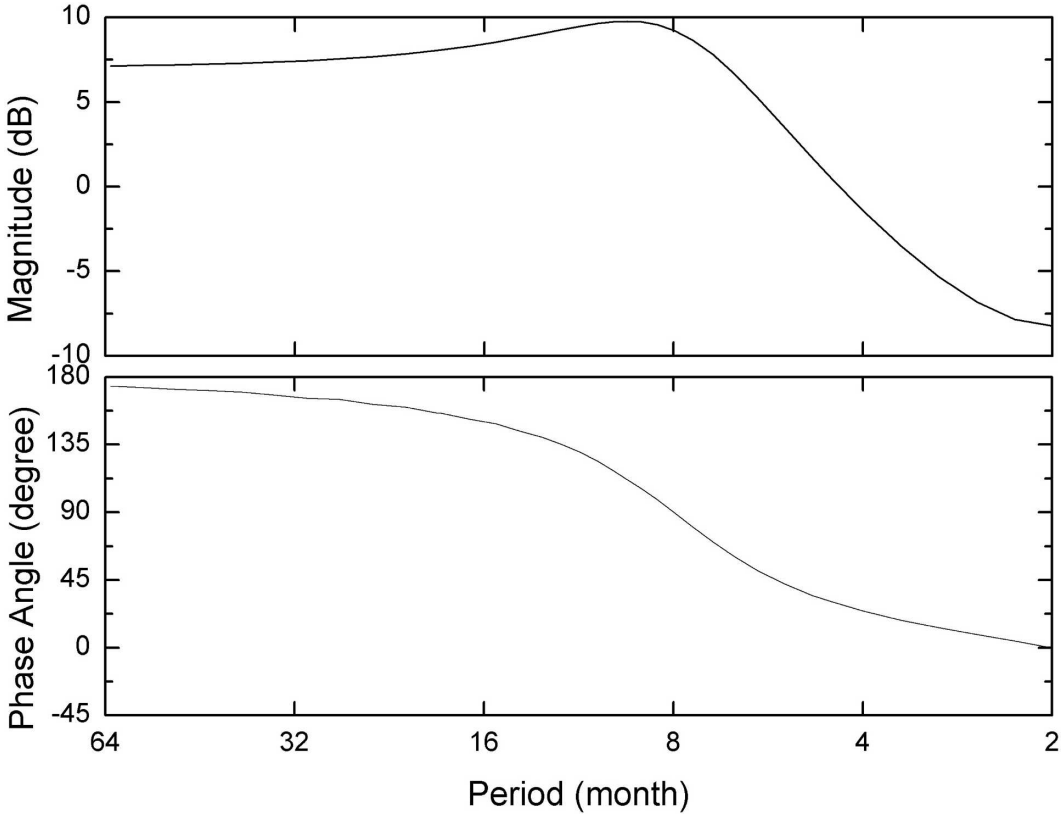

Figure 8. System response functions of precipitation as driven by external disturbances of vegetation (closed-loop model).

corresponding characteristics of the open-loop model (Figure 6). For instance, positive vegetation anomalies (without corresponding water input) will tend to decrease soil moisture (i.e., "V_{soil}" of Figure 6) and as such they will have negative impacts on precipitation as well (Figure 8).

Together, the results of Figures 7 and 8 indicate that vegetation feedbacks add additional variability to precipitation such that it has red spectra as well. To verify this feature in the observations, we calculate power spectra of observed precipitation anomalies based on the CPC U.S. UNIFIED Precipitation datasets (Higgins et al. 1996; Higgins et al. 2000). Before the power spectra are calculated, precipitation anomalies at each grid point are normalized to have unit variance, such that the spectra of all the grid points can be averaged to represent the mean power spectra for the North American Grasslands (Figure 9, dark solid line). As shown, the mean power spectra of the observed anomalies have higher magnitudes (about −4 dB) at time scales longer than 16 months, but lower magnitudes (about −5.5 dB) at periods of 4 months or shorter (Figure 9, dark solid line). The standard deviations of the mean power spectra (averaged over 2700 grid points) are about 0.03 dB at all frequencies; therefore, a magnitude difference of 1.5 dB indicates red spectra of precipitation variations in a statistically significant fashion.

The observed red spectra of precipitation anomalies can be reproduced by model

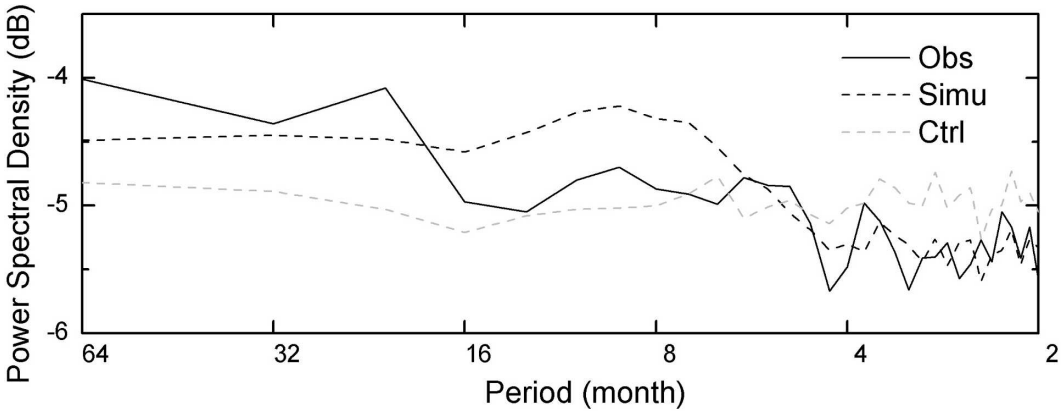

Figure 9. Mean power spectra of observed precipitation and model simulations. "Obs": observations compiled from the CPC U.S. UNIFIED precipitation datasets (Higgins et al. 2000); "Simu": simulations with the closed-loop model with the feedback coefficient set to $\theta/2$; "Ctrl": random inputs used for the model simulation.

simulations (Figure 9, dash lines). Results indicate that when the model uses a feedback coefficient of $\theta/2$ (Table 2), the power spectra of the simulated precipitation (Figure 9, dark dash line) show a similar magnitude range as the observed values (Figure 9, dark solid line), while the spectra of the random inputs are essentially "flat" (Figure 9, gray dash line). When the model uses the full value of θ, the output precipitation has larger magnitude differences between high and low frequencies (not shown). The overestimated red spectra of the model simulations may be due to the fact that the strength of land–atmosphere interactions in the observed system has monthly/seasonal variability (W1), which is not included in the model (here all values are constant through the entire simulation). For the same reason, the model may also overestimate the spectral magnitudes at 8–16-month time scales (Figure 9).

The red power spectra of the observed precipitation shown in Figure 9 do not rule out the possibility that they may be induced by other external processes at interannual or longer time scales (e.g., ocean–atmosphere interactions). To address this problem, we divide the observed monthly precipitation anomalies into growing season months (GS; March–October) and nongrowing season months (NonGS; September–April), and calculate the power spectra for the two time windows separately (Figure 10, top). The two 8-month periods are defined to facilitate the calculation, and the overlap between them does not substantially influence the results (not shown). For comparison, we also divide the model simulations and the random inputs into 8-month segments and recalculate their power spectra, respectively (Figure 10, bottom).

As shown (Figure 10, top), the power spectra of the observed GS precipitation anomalies have higher magnitude (−4.7 dB) at the 8-month period and have lower magnitudes (about −5.2 dB) at the 4-month or shorter time scales, which is consistent with the red characteristics of the full spectra in the same frequency ranges (Figure 9; also shown in gray solid line in Figure 10, top). On the other hand, the

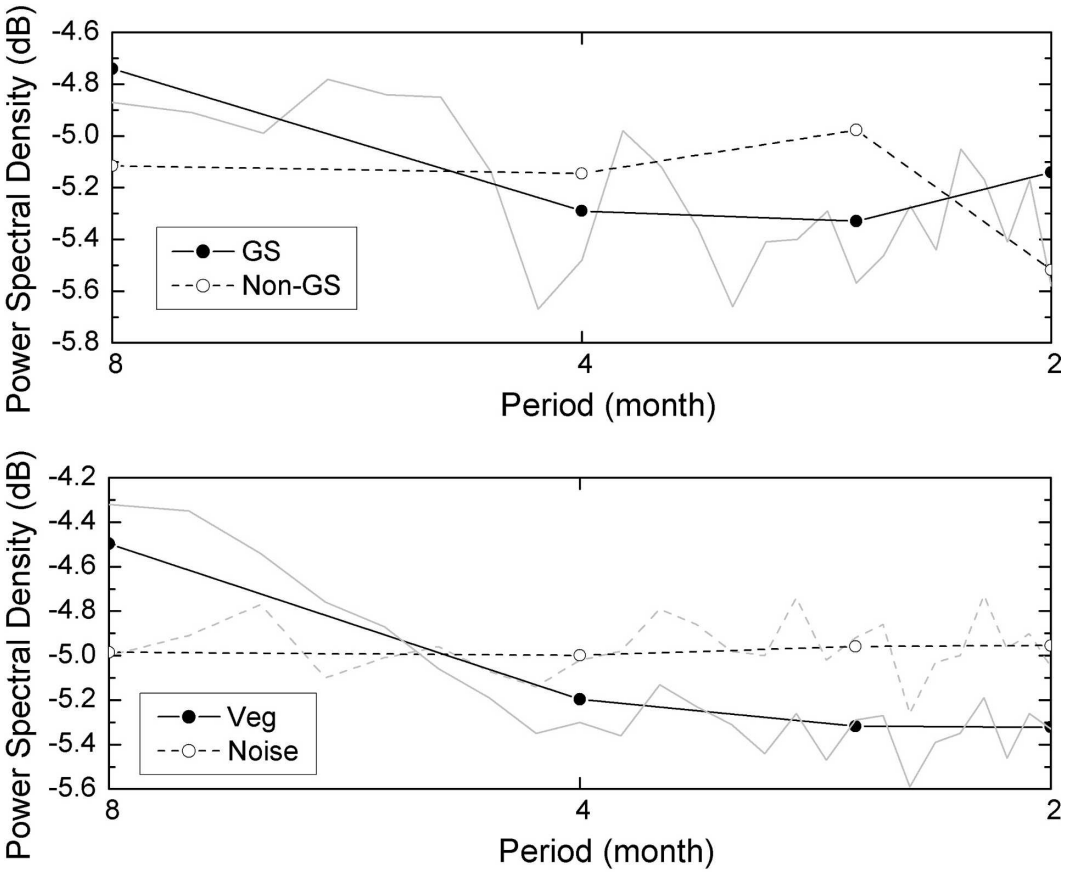

Figure 10. (top) Power spectra of observed precipitation (taken from the CPC UNIFIED datasets) during the GS (March–October, dark solid line) and the NonGS (September–April, dark dashed line). The gray line shows the continuous power spectra for the observations as in Figure 9. (bottom) Power spectra of simulated precipitation (solid lines) and the random inputs. The dark lines show values calculated based on 8-month segments of simulations and controls, and the gray lines are the corresponding continuous spectra from the simulations as shown in Figure 9.

power spectra of observed NonGS precipitation anomalies have almost the same magnitudes (about −5.1 dB) at periods of 8, 4, and 8/3 months, while there is a magnitude drop (about −5.5 dB) at the 2-month period (Figure 10, top). Comparing the spectral characteristics of the observed precipitation anomalies with those of the model simulations, it indicates qualitative agreement between the observed GS anomalies and the simulated precipitation, as well as qualitative agreement between the NonGS anomalies and the random inputs (Figure 10, bottom). Therefore, these results suggest that land surface feedbacks during the growing season represent an important source for the red spectra of the precipitation anomalies shown in Figure 9, which is not present during the nongrowing season.

However, results of Figure 10 cannot be uniquely attributed to the influence of vegetation upon precipitation variability. In fact, the feedback function of Equation

(6) is not the only process that can lead to the red shift in the power spectra of precipitation. For example, removing the vegetation terms from Equation (6) gives

$$P'_t = \theta P'_{t-1} + \varepsilon_t, \tag{12}$$

which can also induce red spectral characteristics of precipitation that are similar to those observed (not shown). Equation (12) can be understood as a direct interaction between soil and the atmosphere (e.g., via evaporation), without any influence of vegetation upon soil–atmosphere water exchanges. Theoretically, the principal difference between Equation (6) and Equation (12) is that vegetation feedbacks [Equation (6)] can introduce oscillatory variability in precipitation (e.g., Figure 7 and Figure 8), while direct soil moisture–precipitation variations [as contained in Equation (12)] cannot. However, because vegetation feedbacks are strong only in certain seasons during the year (e.g., summer), identifying such oscillatory characteristics directly from the power spectra of Figure 9 remains difficult. Therefore, other metrics are required to further analyze the role of vegetation in influencing precipitation, which we discuss in the following section.

5. Model experiments

We conduct Monte Carlo experiments to determine which candidate models best capture the observed summertime precipitation–vegetation interactions. The three candidates are the open-loop model [Equation (5); "OPEN"], the closed-loop model with the feedback function described by Equation (6) ("VEG"), and the closed-loop model in which the feedback function is given by Equation (12) ("AR1"). These models have the same model component to describe vegetation variability [i.e., Equation (5)], but they differ from one another only in the ways they treat precipitation: in the OPEN model precipitation variations are simply assumed to be white noise; in the VEG model precipitation variability depends on the preceding status of both precipitation and vegetation; and in the AR1 model precipitation is only related to its own preceding status, and not to vegetation.

In each model experiment, the external climate forcing and the external disturbances to vegetation are represented by two random time series, which have a Gaussian distribution and standard deviations of 0.7 (mm day^{-1}, precipitation) and 0.02 (NDVI), respectively. The simulated vegetation (V) and precipitation (P) are truncated (with the first 500 values discarded) to 11 628 samples (i.e., 12 months × 19 yr × 51 pixels), which is the length of the panel data for the North American Grasslands (W1). As such, these model simulations can be analyzed in the same way that the observational data are analyzed (W1). The model experiments are repeated 10 000 times to estimate the mean state of each model as well as the corresponding intraseasonal evolution.

We compare the model simulations with the observations using the autocorrelations of monthly vegetation and precipitation anomalies, as well as the lagged cross correlations between them (Figure 11; correlations of the observed data are averaged over July–September). Overall, all the models capture the observed vegetation variability. Simulations and observations show that the autocorrelations of vegetation (NDVI) decrease from positive values (e.g., 0.7) to negative values (e.g., −0.2) as the time lag increases to 4 months (Figure 11a), which is an indicator of oscillatory variability in the vegetation anomalies (W1). Also, all models and

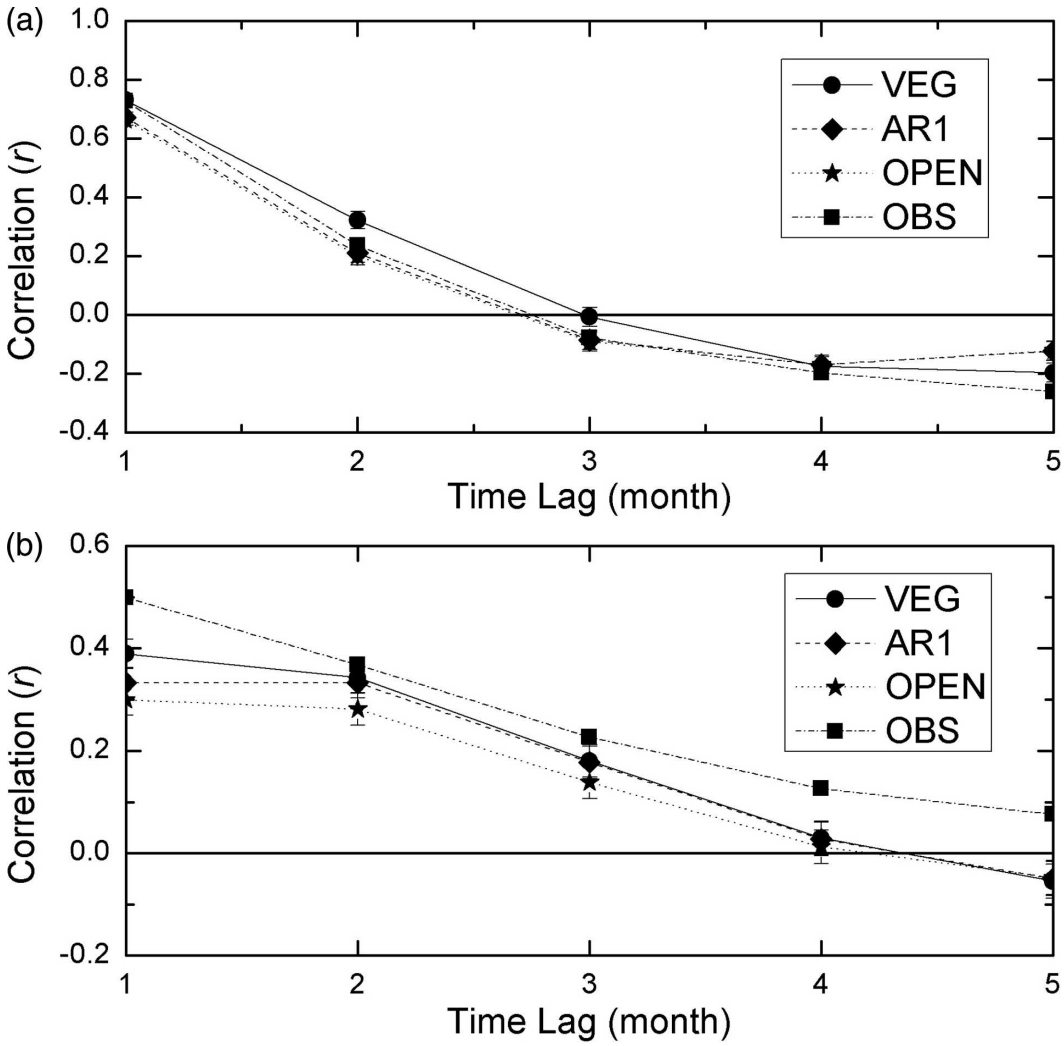

Figure 11. Autocorrelations and lagged correlations of/between anomalies of vegetation and precipitation. (a) Correlations between *V*(*t*) and *V*(*t*–lag), (b) correlations between *V*(*t*) and *P*(*t*–lag), (c) correlations between *P*(*t*) and *P*(*t*–lag), and (d) correlations between *P*(*t*) and *V*(*t*–lag). VEG stands for the closed-loop model with vegetation feedbacks (Equation (6)), AR1 denotes the closed-loop model with precipitation related only to its own preceding status (but not vegetation), OPEN is the open-loop model, and OBS indicates observations that are averaged over the late summer (July–September).

observations indicate that the positive correlations between vegetation and the preceding precipitation variations decrease as time lag increases (Figure 11b).

On the other hand, the models differ in describing the variability of precipitation. As shown in Figure 11c, autocorrelations of observed precipitation decrease from positive values (~0.12, at the 1-month lag) to slightly negative values (–0.05, at lags longer than 3 months; Figure 11c, "OBS"). At the same time, cross cor-

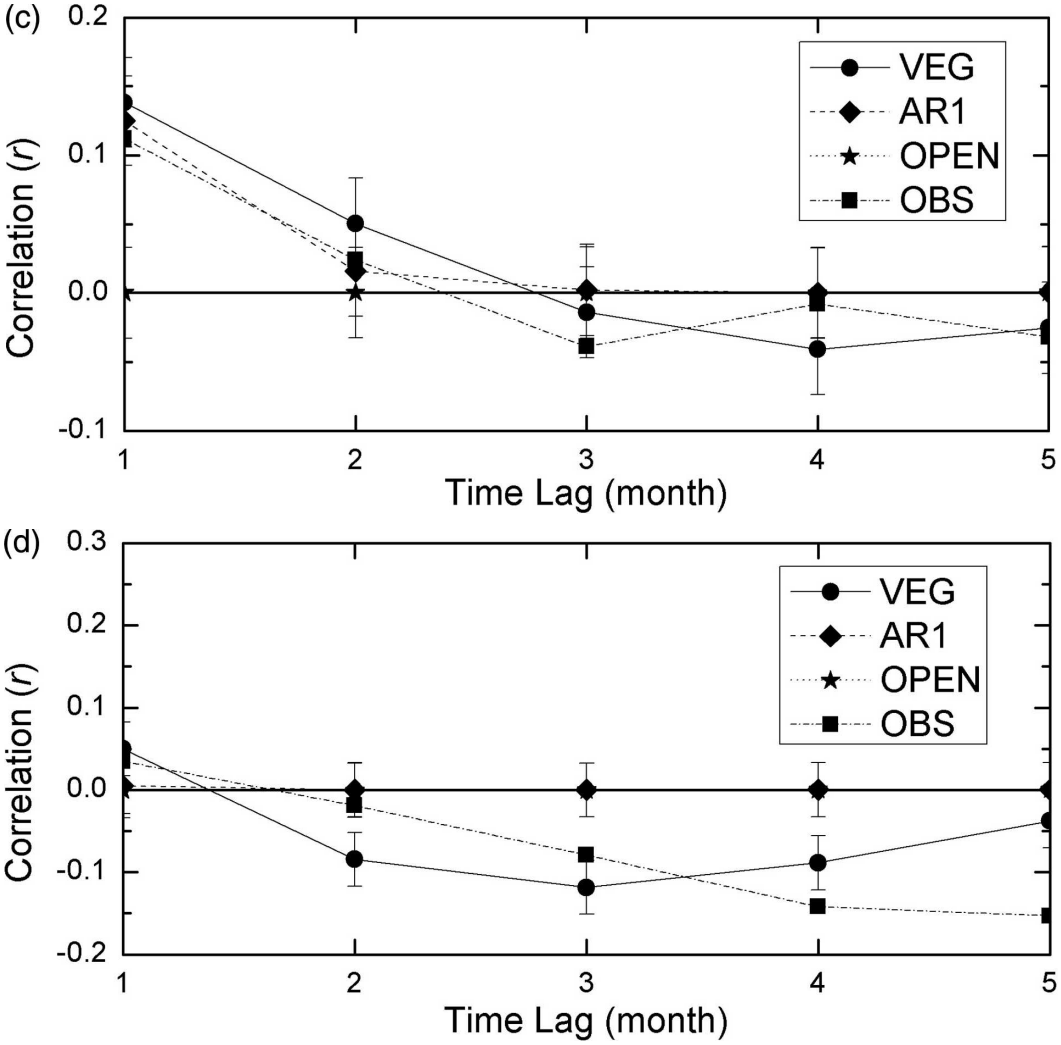

Figure 11. (*Continued*)

relations between current precipitation (P'_t) and lagged vegetation ($V'_{t-\text{lag}}$) have negative values as time lag increases (Figure 11d, OBS). Of the model simulations, only the VEG model captures both these observed characteristics (Figure 11c and Figure 11d, VEG). In contrast, because precipitation in the OPEN model is random, it cannot be predicted either by preceding values of itself or those of vegetation. As such, it has essentially zero autocorrelations and lagged cross correlations (Figure 11c and Figure 11d, OPEN). The AR1 model captures the decreasing trajectory of the autocorrelations of precipitation anomalies; however, these autocorrelations converge to zero at the 3-month lag and do not become negative (Figure 11c, AR1). Also, vegetation in the AR1 model shows no information about future precipitation (Figure 11d, AR1). Together, these results indicate that the VEG model, which incorporates the feedback of vegetation upon the atmosphere, best captures the observed statistical precipitation–vegetation interaction characteristics.

It is noted that the correlation structures of model simulations are likely to deviate from the observations at long time lags (Figure 11). For example, simulations show that correlations between vegetation (V'_t) and lagged precipitation ($P'_{t-\text{lag}}$) become slightly negative at the 5-month lag, while the observations do not (Figure 11b). Also, the negative correlations between simulated precipitation (P'_t) and vegetation ($V'_{t-\text{lag}}$) show a recovering tendency at lags longer than 3 months, while the observations indicate a further decrease (Figure 11d). These differences may reflect the seasonal variations of the precipitation–vegetation interactions. Additional analyses indicate that at the beginning of the growing season (e.g., April and May) vegetation is less dependent on precipitation and is more strongly related to temperature (not shown); in this sense, higher vegetation anomalies may be associated with warmer temperatures but less rainfall during the cooler early growing season months. Because both factors have negative impacts on soil moisture (e.g., Figure 3 and Figure 5), they suggest that higher vegetation in spring may be followed by precipitation anomalies that are lower than expected in summer (negative correlation; Figure 11d, OBS). In the same way, higher precipitation in spring may precede higher-than-expected vegetation in summer (positive correlation; Figure 11b, OBS) because the consumption of soil water is delayed until later in the growing season.

Finally, we verify these model simulations by testing Granger causal relationships from vegetation to precipitation, which examines whether lagged vegetation anomalies contain information to predict current precipitation variability (W1). In particular, for the case of 4-month lags, we test how the mean (V'_{mean}) and the trend (V'_{diff}) of vegetation anomalies over the preceding months contribute to such relationships (W1). From W1, V'_{mean} and V'_{diff} are defined by

$$V'_{\text{mean}} = \sum_{l=1}^{4} V'_{t-l}/4, \quad V'_{\text{diff}} = \sum_{l=1}^{2} V'_{t-l}/2 - \sum_{l=3}^{4} V'_{t-l}/2. \tag{13}$$

Of the total 10 000 experiments, the results indicate that 96% of VEG simulations have a significant causal relationship from vegetation to precipitation, while the corresponding numbers for both OPEN and AR1 models are about 4%. In addition, in 99% of the VEG experiments the sign associated with V'_{mean} is negative, and in 84% of the VEG experiments, the sign associated with V'_{diff} is positive. These results indicate that higher mean values or/and decreasing trends of vegetation variations are likely to precede lower precipitation anomalies and hence are consistent with the findings of W1 based upon the *observed* data. Furthermore, it is found that when the model (VEG) is simulated only with the external climate forcing, in which all the information of vegetation is derived only from precipitation, the significant causal relationships disappear (not shown). These experiments further indicate that a system in which there is negligible influence of vegetation on precipitation could not spuriously produce the observed results found in W1.

6. Conclusions

This paper develops a simple stochastic model to quantitatively investigate interactions between anomalous precipitation and vegetation over the North American Grasslands. Based on characteristics of biohydrological processes in this semiarid environment, the model has components to describe the water-related

vegetation variability, the long-term balance of soil moisture, and the local soil moisture–precipitation feedbacks. These dynamic relationships are quantified by five physically meaningful parameters, which describe the persistence rate of vegetation, precipitation, and soil moisture, as well as the short-term/long-term responses of vegetation to precipitation forcing. To facilitate the comparison with the observational analysis (W1), the model is represented in two linear difference equations, with a focus on how precipitation drives variations in vegetation (the open-loop model), and how vegetation signals feed back to the atmosphere (the feedback equation). This representation allows the system parameters to be readily estimated from the observational data.

Analyses indicate that the open-loop model, which represents the variability of vegetation driven by precipitation, captures two principal characteristics of the observed vegetation dynamics. First, the model indicates that vegetation has a "red" response function to precipitation forcing; that is, vegetation responds more actively to low-frequency precipitation variations but does not respond to rapid disturbances. Second, the model indicates that the system has intrinsic oscillatory variability, which is induced by interactions between vegetation and soil moisture. With the estimated system parameters, this oscillation frequency is calculated to be 0.76 rad month^{-1}, representing a period of about 8 months, which is consistent with the analysis of W1.

Analyses of the closed-loop model indicate that vegetation signals can impart similar spectral signatures on the variability of precipitation when they feed back to the atmosphere. The frequency-response functions of the model show that the magnitude of precipitation is slightly enhanced at low frequencies (e.g., periods $\geq$8 months) but damped at high frequencies (e.g., periods $\leq$4 months), regardless of the external forcing coming from the climate side or the vegetation side. Such red frequency characteristics are verified by the power spectra of observed precipitation datasets and the model simulations. The role of vegetation in influencing precipitation variability is further verified by Monte Carlo experiments. Only when the vegetation feedback is incorporated can the model simulations reproduce characteristics of observed covariability between summertime precipitation and vegetation anomalies, as represented by the lagged correlations and the Granger causal relationships. These relationships indicate that higher mean values and/or decreasing trends of vegetation anomalies are likely followed by lower precipitation anomalies, in agreement with observed results (W1).

More important than just replicating the characteristics of the observed precipitation–vegetation interactions, the dynamic aspects of the model provide insights for the understanding of the physical mechanisms of the system. For example, the red response functions of vegetation reflect the fact that the short-term production of vegetation is lower than its long-term balance with precipitation. Therefore, it takes time for vegetation to fully respond to a precipitation impulse; in other words, an impulse of precipitation will generate variations of vegetation in the following months and not simply during the precipitating month. At the same time, because preceding vegetation anomalies also consume water, this response process is also regulated by the persistence rate of vegetation and soil moisture. Depending on the values of these parameters, the adjustments of the system can either be oscillatory or nonoscillatory, although the parameter space tends to be dominated by oscillatory behavior.

The model also helps to clarify the role of vegetation in regulating soil moisture and precipitation. Because vegetation represents the principal pathway in which water is depleted from soil, from the perspective of soil water balance, vegetation-induced evapotranspiration acts as a negative feedback to help maintain the stability of the system. For the open-loop model, such equilibrium of the system is reached only when the incoming water (precipitation) is exactly balanced by the outgoing water (evapotranspiration), such that soil moisture becomes invariant and the long-term relationship between vegetation and precipitation is established. Deviations arising from either precipitation or vegetation anomalies will be restrained by this negative feedback process to gradually return to their equilibrium status. For the closed-loop model, although vegetation prompts the water exchange between land and atmosphere at long time scales, it also enhances the diffusion of water to the atmosphere and implicitly removes it from the region. For this reason, without increases in incoming water (via precipitation), increases of vegetation (i.e., external disturbances to vegetation) will have negative overall impacts on soil moisture and precipitation. This result explains why positive vegetation anomalies at the beginning of the growing season, probably prompted by warmer temperatures, may precede drier conditions later in the summer (W1).

Finally, it is important to note that we do not argue that the model developed in this paper (as well as the physical mechanisms it represents) is the only way that vegetation influences precipitation variability. Indeed, because the model is mainly developed to provide a physically meaningful explanation for the observed intraseasonal covariability between vegetation and climate anomalies (W1), it has simplified many important processes (e.g., through the albedo feedback; Brovkin et al. 1998) that can significantly influence climate variability at long time scales. The statistical results and the stochastic model of this study are also restrained by the methodologies and, in particular, by the datasets used in the analyses. Therefore, it is recognized that findings of this study need to be further investigated by dedicated observational and process-based approaches in the future.

Acknowledgments. This work was supported in part by the NASA Earth Science Enterprise. The views expressed herein are those of the authors and do not necessarily reflect the views of NASA. The authors are thankful to Dr. Guiling Wang and another anonymous reviewer for their constructive comments and suggestions. CMAP precipitation data were provided by the NOAA–CIRES ESRL/PSD Climate Diagnostics branch, Boulder, Colorado, from their Web site (http://www.cdc.noaa.gov/). CPC U.S. UNIFIED Precipitation data were provided by the NOAA–CIRES ESRL/PSD Climate Diagnostics branch, Boulder, Colorado, from their Web site (http://www.cdc.noaa.gov/). We also would like to thank Dr. C. J. Tucker for providing the GIMMS NDVI data.

Appendix

Model Derivation

1.1. Objective

The model in the paper was directly developed in the form of *linear difference equations* to describe relationships among *anomalies* of vegetation, soil moisture,

and precipitation. However, interactions among these fields (their *full* values) are known to be *nonlinear* and are typically studied using physically based models in the literature. As such, a question naturally arises: Is there a link between the stochastic model of this study and those physical models? This appendix is intended to address this question.

1.2. The general model

In the first step, we want to show that generally, climate–vegetation interactions in a semiarid environment may be described by the following form:

$$dV/dt = -a(V, S)V + b(V, S)S, \tag{A1}$$

$$dS/dt = P - c(V, S)S. \tag{A2}$$

$$P = \theta S + f_p, \tag{A3}$$

where V, S, and P represent vegetation (e.g., NDVI), soil moisture, and precipitation, respectively; f_p stands for the external forcing of precipitation; and a, b, c, and θ represent the parameters of the system. Note that a, b, and c are treated as nonnegative *functions* of vegetation and soil moisture. To keep the model simple, θ is still assumed to be a constant coefficient (see below for discussions).

Equation (A1) describes vegetation dynamics. It is based on the notion that vegetation growth is determined by the balance between the loss of biomass (through respiration or metabolism) and the production of vegetation (through photosynthesis). Because the environment is arid, it is assumed that vegetation production is mainly regulated by soil moisture (Churkina and Running 1998). Therefore, the parameters a and b can be interpreted as the rate of vegetation loss and of production, respectively. This form of the biomass equation is generally utilized in dynamic vegetation models (e.g., Foley et al. 1996; Dickinson et al. 1998). To illustrate with an example, we rewrite the vegetation model in Zeng et al. (1999) as follows:

$$dV/dt = -V/\tau + \alpha[1 - e^{-kL(V)}]\beta(S), \tag{A4}$$

where τ is understood as the time constant of vegetation, α is the carbon assimilation coefficient, k is a photosynthesis coefficient, $L(V)$ is a plant leaf area index function, and $\beta(S)$ is a function of soil moisture (Zeng et al. 1999). By comparing Equation (A1) and Equation (A4), it is clear that the former represents a general form of the latter.

Equation (A2) describes the balance of soil moisture. This equation is based upon the assumption that in the arid environment, soil moisture is mainly balanced by precipitation (P) and evapotranspiration (ET); that is,

$$dS/dt = P - \mathrm{ET}. \tag{A5}$$

Equation (A5) is generally known as a simple bucket model. Previous studies (e.g., Mintz and Serafini 1984; Serafini and Sud 1987; Yamaguchi and Shinoda 2002) suggest that evapotranspiration may be modeled as

$$\mathrm{ET} = \frac{\mathrm{PET}}{f} S, \tag{A6}$$

where f is some function of the soil properties, and PET represents the potential evapotranspiration.

Potential evapotranspiration (PET) over vegetated surface can be modeled using the Penman–Monteith equation (Penman 1953; Monteith 1965); however, this requires much more information than is available from datasets used here. Instead, we assume that the ideal PET can be optimally approximated by some function of vegetation and soil moisture [denoted as $c(V,S)$]; that is,

$$\frac{\mathrm{PET}}{f} \doteq c(V, S). \tag{A7}$$

The parameter function c can be understood as the turnover rate of soil moisture. From Equation (A5) to Equation (A7), we get the general equation of soil water balance, Equation (A2).

Equation (A3) describes the soil moisture–precipitation feedbacks in the model. It is based upon the notion that precipitation over large regions is supplied by the influx of water vapor from outside the given region [i.e., f_p in Equation (A3)], and by the local water flux evapotranspirated from the soil (Rodrigues-Iturbe et al. 1991a). Therefore, the parameter θ in Equation (A3) can be interpreted as the proportion of soil moisture that contributes to local precipitation. Because this parameter describes only a statistical relationship, and because ultimately we want to represent such a relationship in a linear form, we assume θ is a constant coefficient to keep the equation simple. (In other cases we can use the techniques described below to linearize this equation.)

1.3. Linearization

To linearize the general model proposed above, we rewrite the system variables as sums of their long-term means (i.e., climatologies) and deviations from the means (i.e., anomalies), that is,

$$\begin{cases} V = \overline{V} + V' \\ S = \overline{S} + S' \\ P = \overline{P} + P' \\ f_p = \bar{f}_p + f'_p, \end{cases} \tag{A8}$$

where $\overline{V}$, $\overline{S}$, $\overline{P}$, and $\bar{f}_p$ represent the climatologies of the system variables, and V', S', P', and f'_p represent the corresponding anomalies. Generally, it is assumed that there is an equilibrium among the climatologies of the system, such that

$$\begin{cases} d\overline{V}/dt = -a(\overline{V}, \overline{S})\overline{V} + b(\overline{V}, \overline{S})\overline{S} = 0 \\ d\overline{S}/dt = \overline{P} - c(\overline{V}, \overline{S})\overline{S} = 0 \\ \overline{P} = \theta\overline{S} + \bar{f}_p. \end{cases} \tag{A9}$$

This assumption can be made because, simply speaking, once the external climate forcing (e.g., f_p) takes its climatological value, the rest of the system variables would be expected to reach their climatological values as well.

Based on Equation (A8), we also rewrite the general model Equation (A1)–Equation (A3) as follows:

$$\begin{cases} d(\overline{V}+V')/dt = -a(\overline{V}+V', \overline{S}+S')(\overline{V}+V') + b(\overline{V}+V', \overline{S}+S')(\overline{S}+S') \\ d(\overline{S}+S')/dt = (\overline{P}+P') - c(\overline{V}+V', \overline{S}+S')(\overline{S}+S') \\ (\overline{P}+P') = \theta(\overline{S}+S') + (\overline{f}_p + f'_p). \end{cases} \tag{A10}$$

The basic method to linearize Equation (A10) is to 1) expand the parameters a, b, and c as linear functions around their climatological values ($\overline{V}$, $\overline{S}$); 2) neglect all the second-order anomaly terms (V', S', and P'); and 3) eliminate the long-term equilibrium relationships [Equation (A9)] from the equations. The first step can be done with

$$\begin{cases} a(\overline{V}+V', \overline{S}+S') \doteq a(\overline{V}, \overline{S}) + \left.\dfrac{\partial a}{\partial V}\right|_{\overline{V},\overline{S}} V' + \left.\dfrac{\partial a}{\partial S}\right|_{\overline{V},\overline{S}} S' \\ b(\overline{V}+V', \overline{S}+S') \doteq b(\overline{V}, \overline{S}) + \left.\dfrac{\partial b}{\partial V}\right|_{\overline{V},\overline{S}} V' + \left.\dfrac{\partial b}{\partial S}\right|_{\overline{V},\overline{S}} S' \\ c(\overline{V}+V', \overline{S}+S') \doteq c(\overline{V}, \overline{S}) + \left.\dfrac{\partial c}{\partial V}\right|_{\overline{V},\overline{S}} V' + \left.\dfrac{\partial c}{\partial S}\right|_{\overline{V},\overline{S}} S'. \end{cases} \tag{A11}$$

Following the steps described above, these equations give

$$dV'/dt = -\overline{a}V' + \overline{b}S', \tag{A12}$$

$$dS'/dt = P' - \overline{c}_S S' - \overline{c}_V V', \tag{A13}$$

$$P' = \theta S' + f'_p, \tag{A14}$$

where $\overline{a}$, $\overline{b}$, $\overline{c}_S$, and $\overline{c}_V$ are constant coefficients (i.e., the *Jocobians*; Glendinning 1994), and are given by

$$\begin{cases} \overline{a} = a(\overline{V}, \overline{S}) + \left.\dfrac{\partial a}{\partial V}\right|_{\overline{V},\overline{S}} \overline{V} - \left.\dfrac{\partial b}{\partial V}\right|_{\overline{V},\overline{S}} \overline{S} \\ \overline{b} = b(\overline{V}, \overline{S}) + \left.\dfrac{\partial b}{\partial S}\right|_{\overline{V},\overline{S}} \overline{S} - \left.\dfrac{\partial a}{\partial S}\right|_{\overline{V},\overline{S}} \overline{V} \\ \overline{c}_S = c(\overline{V}, \overline{S}) + \left.\dfrac{\partial c}{\partial S}\right|_{\overline{V},\overline{S}} \overline{S} \\ \overline{c}_V = \left.\dfrac{\partial c}{\partial V}\right|_{\overline{V},\overline{S}} \overline{S} \end{cases}. \tag{A15}$$

Therefore, Equations (A12), (A13), and (A14) represent the linear form of the general model, which describes interactions among *anomalies* of the system variables.

1.4. Difference equations

To facilitate the discussion, the model derived in the paper (in difference equations) is rewritten here as

$$V'_t = \alpha V'_{t-1} + \beta S'_{t-1}, \tag{A16}$$

$$S'_t = \sigma S'_{t-1} + P'_t - \frac{1}{\gamma} V'_t, \tag{A17}$$

$$P'_t = \theta S'_{t-1} + \varepsilon_t. \tag{A18}$$

The correspondence between Equation (A16)–Equation (A18) and Equation (A12)–Equation (A14) is apparent. However, there are also some subtle differences. For instance, the coefficients of the difference equations are generally different from those of the original differential equations because coefficients in the discrete time domain implicitly include information about the data-sampling periods [i.e., the "*dt*" term in Equations (A12)–(A14)]. Also, Equation (A17) introduces some instantaneous effects of precipitation and vegetation on soil moisture, which are not exactly described by Equation (A13). In addition, the time lag of the soil moisture term in Equation (A18) is adjusted. Such adjustments are made because the observational data are generally smoothed over a fixed time period, which may affect the time sequences of the relationships among them. For example, the instantaneous relationships commonly seen in statistical models are rarely described by differential equations. Generally, these adjustments allow the model to better describe the statistical relationships among the observational data and at the same time to preserve the physical meaning of the model and its parameters.

References

Alcock, J., 2003: Positive feedback and system resilience from graphical and finite-difference models: The Amazon ecosystem—An example. *Earth Interactions,* **7**. [Available online at http://EarthInteractions.org.]

Brovkin, V., M. Claussen, V. Petoukhov, and A. Ganopolski, 1998: On the stability of the atmosphere-vegetation system in the Sahara/Sahel region. *J. Geophys. Res.,* **103,** 31 613–31 624.

Churkina, G., and S. W. Running, 1998: Contrasting climatic controls on the estimated productivity of global terrestrial biomes. *Ecosystems,* **1,** 206–215.

Delire, C., J. A. Foley, and S. Thompson, 2004: Long-term variability in a coupled atmosphere–biosphere model. *J. Climate,* **17,** 3947–3959.

Dickinson, R. E., M. Shaikh, R. Bryant, and L. Graumlich, 1998: Interactive canopies for a climate model. *J. Climate,* **11,** 2823–2836.

Diebold, F. X., and R. S. Mariano, 1995: Comparing predictive accuracy. *J. Bus. Econ. Stat.,* **13,** 253–263.

Foley, J. A., I. C. Prentice, N. Remankutty, S. Levis, D. Pollard, S. Sitch, and A. Haxeltine, 1996: An integrated biosphere model of land surface processes, terrestrial carbon balance, and vegetation dynamics. *Global Biogeochem. Cycles,* **10,** 603–628.

Friedl, M. A., and Coauthors, 2002: Global land cover mapping from MODIS: Algorithms and early results. *Remote Sens. Environ.,* **83,** 287–302.

Glendinning, P., 1994: *Stability, Instability, and Chaos: An Introduction to the Theory of Nonlinear Differential Equations.* Cambridge University Press, 388 pp.

Granger, C. W. J., 1969: Investigating causal relations by econometric models and cross-spectral methods. *Econometrica,* **37,** 424–438.

——, 1980: Testing for causality: A personal viewpoint. *J. Econ. Dyn. Control,* **2,** 329–352.

——, and L. Huang, 1997: Evaluation of Panel Data Models: Some suggestions from time series. Department of Economics, University of California, San Diego, 29 pp.

Heck, P., D. Luthi, and C. Schar, 1999: The influence of vegetation on the summertime evolution of European soil moisture. *Phys. Chem. Earth,* **24,** 609–614.

——, ——, H. Wernli, and C. Schar, 2001: Climate impacts of European-scale anthropogenic vegetation changes: A sensitivity study using a regional climate model. *J. Geophys. Res.,* **106,** 7817–7835.

Higgins, R. W., J. E. Janowiak, and Y.-P. Yao, 1996: *A Gridded Hourly Precipitation Data Base for the United States (1963–1993).* NCEP/Climate Prediction Center Atlas No. 1, National Centers for Environmental Prediction, 46 pp.

——, W. Shi, E. Yarosh, and R. Joyce, 2000: *Improved US Precipitation Quality Control System and Analysis.* NCEP/Climate Prediction Center Atlas No. 7, National Centers for Environmental Prediction, [Available online at http://www.cpc.ncep.noaa.gov/research_papers/ncep_cpc_atlas/7/index.html.]

Koster, R. D., and Coauthors, 2004: Regions of strong coupling between soil moisture and precipitation. *Science,* **305,** 1138–1140.

Manabe, S., 1969: Climate and the ocean circulation. 1. The atmospheric circulation and the hydrology of the earth's surface. *Mon. Wea. Rev.,* **97,** 739–774.

Mintz, Y., and Y. Serafini, 1984: Global fields of monthly normal soil moisture, as derived from observed precipitation and an estimated potential evapotranspiration. Part V, Final Scientific Rep. under NASA Grant NAS 5-26, Dept. of Meteorology, University of Maryland, 182 pp.

Monteith, J. L., 1965: Evaporation and environment. *Symp. Soc. Exp. Biol.,* **19,** 205–234.

Myneni, R. B., C. D. Keeling, C. J. Tucker, G. Asrar, and R. R. Nemani, 1997: Increased plant growth in the northern high latitudes from 1981–1991. *Nature,* **386,** 698–702.

——, C. J. Tucker, G. Asrar, and C. D. Keeling, 1998: Interannual variations in satellite-sensed vegetation index data from 1981 to 1991. *J. Geophys. Res.,* **103** (D6), 6145–6160.

Nemani, R. R., and Coauthors, 2003: Climate-driven increases in global terrestrial net primary production from 1982 to 1999. *Science,* **300,** 1560–1563.

Penman, H. L., 1953: The physical bases of irrigation control. *Rep. 13th Int. Hort. Cong.,* **2,** 913–923.

Reid, J. G., 1983: *Linear System Fundamentals: Continuous and Discrete, Classic and Modern.* McGraw-Hill, 484 pp.

Rodriguez-Iturbe, I., D. Entekhabi, and R. L. Bras, 1991a: Nonlinear dynamics of soil moisture at climate scales. 1. Stochastic analysis. *Water Resour. Res.,* **27,** 1899–1906.

——, ——, J.-S. Lee, and R. L. Bras, 1991b: Nonlinear dynamics of soil moisture at climate scales. 1. Chaotic analysis. *Water Resour. Res.,* **27,** 1907–1915.

Serafini, Y. V., and Y. C. Sud, 1987: The time scale of the soil hydrology using a simple water budget model. *J. Climatol.,* **7,** 585–591.

Tucker, C. J., 1979: Red and photographic infrared linear combinations for monitoring vegetation. *Remote Sens. Environ.,* **8,** 127–150.

Wang, G., 2004: A conceptual modeling study on biosphere–atmosphere interactions and its implications for physically based climate modeling. *J. Climate,* **17,** 2572–2583.

Wang, W., B. T. Anderson, N. Phillips, R. K. Kaufmann, C. Potter, and R. B. Myneni, 2006: Feedbacks of vegetation on summertime climate variability over the North American Grasslands. Part I: Statistical analysis. *Earth Interactions,* **10,** in press.

Wever, L. A., L. B. Flanagan, and P. J. Carlson, 2002: Seasonal and interannual variation in evapotranspiration, energy balance and surface conductance in a northern temperate grassland. *Agric. For. Meteor.,* **112,** 31–49.

Woodward, F. I., 1987: *Climate and Plant Distribution.* Cambridge University Press, 174 pp.

Xie, P., and P. A. Arkin, 1997: Global precipitation: A 17-year monthly analysis based on gauge observations, satellite estimates, and numerical model outputs. *Bull. Amer. Meteor. Soc.,* **78,** 2539–2558.

Yamaguchi, Y., and M. Shinoda, 2002: Soil moisture modeling based on multiyear observations in the Sahel. *J. Appl. Meteor.,* **41,** 1140–1146.

Zeng, N., and J. D. Neelin, 2000: The role of vegetation–climate interaction and interannual variability in shaping the African savanna. *J. Climate,* **13,** 2665–2670.

——, ——, W. K.-M. Lau, and C. J. Tucker, 1999: Enhancement of interdecadal climate variability in the Sahel by vegetation interaction. *Science,* **286,** 1537–1540.

——, K. Hales, and J. D. Neelin, 2002: Nonlinear dynamics in a coupled vegetation–atmosphere system and implications for desert–forest gradient. *J. Climate,* **15,** 3474–3487.

Zhou, L., C. J. Tucker, R. K. Kaufmann, D. Slayback, N. V. Shabanov, and R. B. Myneni, 2001: Variations in northern vegetation activity inferred from satellite data of vegetation index during 1981 to 1999. *J. Geophys. Res.,* **106,** 20 069–20 083.